European Polymer Journal 47 (2011) 2266–2276

Contents lists available at SciVerse ScienceDirect

European Polymer Journal

journal homepage: www.elsevier.com/locate/europolj

MACROMOLECULAR NANOTECHNOLOGY

Macromolecular Nanotechnology

Photoluminescence quenching effects of surface-modified gold nanoparticles on side-chain polymers containing pyridyl H-acceptors with various lateral polarities

Hsuan-Chih Chu, Tzung-Chi Liang, Harihara Padhy, Shou-Jen Hsu, Hong-Cheu Lin *

Department of Materials Science and Engineering, National Chiao Tung University, Hsinchu, Taiwan, ROC

ARTICLE INFO

Article history:
Received 29 March 2011
Received in revised form 20 September 2011
Accepted 26 September 2011
Available online 2 October 2011

Keywords:
Fluorescence quenching
Gold nanoparticles
Supramolecualr nanocomposites
Acid and acid-free surfactants

ABSTRACT

In this study, we used photoluminescence (PL) quenching and transmission electron microscopy (TEM) to study the morphological behavior of hydrogen-bonded (H-bonded) supramolecular assemblies of luminescent H-acceptor polymers and H-donor gold nanoparticles (Au NPs). In fluorescence titration experiments, the lateral Me and MeO substituents on the fluorescent H-acceptor side-chain polymers **PBOT1**–**PBOT3** and **PBT1**–**PBT3** exhibited different electron-donating capabilities, thereby inducing different degrees of H-bonding and dipole–dipole interactions, as evidenced by effective fluorescence quenching upon the addition of surface-modified Au NPs bearing acid and acid-free surfactants (**AuSCOOH** and **AuSC10**, respectively). Among all of our tested nanocomposites, the highest Stern–Volmer quenching constant (K_{SV}) was that obtained from the assembly of **AuSCOOH** with the homopolymer **PBOT1**. In addition, we developed fittable exponential equations to predict the values of K_{SV} of other fluorescent polymers (containing various molar ratios of pyridyl conjugated units) when titrated with these NP quenchers. The morphologies observed in the TEM images confirmed that fluorescence quenching resulted from the self-assembly of the supramolecular nanocomposites, mediated by H-bonds between the fluorescent H-acceptors of the polymers and the H-donors of the Au NPs presenting acid-modified surfactants.

1. Introduction

Supramolecular chemistry is a branch of chemistry encompassing systems held together by noncovalent bonds; supramolecular complexes have great potential for use in various rapidly developing fields [1–7]. Recently, directed self-assembly of nanoscale building blocks, mediated by noncovalent interactions (e.g., hydrogen bonding, acid/base proton transfer, electrostatic forces), has led to several interesting developments [8–22]. There is considerable interest in exploiting the fluorescence of conjugated polymers, due to their feasibility for use as highly sensitive chemosensors and biosensors [23–27], which operate based on the different fluorescence quenching abilities induced by supramolecular interactions with particular chemical or biological species [28–31]. Polymers presenting supramolecular receptor groups (e.g., crown ethers, pyridine derivatives and ionic groups) from their side or main chains have been used for the sensing of ions and biological moieties [32–37]. The development of supramolecular assemblies of fluorescent side-chain conjugated polymers, capable of exhibiting either chromogenic or fluorogenic responses in response to noncovalent interactions, has attracted much recent research interest [38–41].

The self-assembly of nanocomposites from nanoparticles (NPs) and fluorescent polymers is a direct means of incorporating the unique physical properties of NPs into

* Corresponding author. Tel.: +8863 5712121x55305; fax: +8863 5724727.
E-mail address: linhc@cc.nctu.edu.tw (H.-C. Lin).

0014-3057/$ - see front matter © 2011 Elsevier Ltd. All rights reserved.
doi:10.1016/j.eurpolymj.2011.09.024

useful functional materials [42–45]. Due to their stability and biocompatibility, gold (Au) NPs surface-modified with organic layers (such as triphenylene and cyclodextrin surfactants) are highly attractive models for the applications of nanocomposites and biosensors [46,47]. Many high-performance fluorescence assays for the optical sensing of important biological ions and molecules have been designed to take advantage of the superquenching ability of Au NPs. Notably, Au NPs can be functionalized with a variety of monolayer structures so that they become soluble in water or organic solvents. Rotello et al. have widely investigated the synthesis and self-assembly of Au NPs with inherent optical properties [16–22]. Starting with thiol-passivated Au NPs, they used thermal ripening and the Murray place exchange reaction to create NPs comprising highly monodisperse cores surface-modified with carboxylic acid-functionalized monolayers. Murray et al. studied the quenching of fluorophores attached to monolayer-protected Au NPs, mediated by electron transfer from the exited fluorophores to the Au NPs [48]. Direct binding between a fluorophore and a metal surface often results in quenching of the fluorophore's excited states through both energy transfer and electron transfer processes [49]. Moreover, the Au NPs in the quenched nanocomposites (containing fluorophores) can be replaced by other metal ions to different degrees, as a result of stronger re-coordination or re-complexation of the metal ions with the fluorophores, thereby restoring the fluorescence of the chromophores and providing chemosensors that function through a two-stage self-assembly process [50,51]. In addition, the Au NPs of quenched nanocomposites have also been reacted with reduced glutathione in the presence of a glutathione reductase enzyme; the subsequent recovery of the fluorescence of the chromophores allowed these systems to behave as biosensors [52].

In a previous study, we explored the supramolecular assembly of nanocomposites of fluorescent copolymers presenting proton acceptors (H-acceptors) and surface-functionalized Au NPs presenting proton donors (H-donors), in terms of both their photoluminescence (PL) quenching phenomena and transmission electron microscopy (TEM) morphologies [53]. Competition between the H-donors of the acid pendent units of the copolymers and the acid surfactants of the Au NPs complicated that investigation of those supramolecular nanocomposites. Therefore, in this study, we replaced the acidic H-donor moieties of the previous self–H-bonded copolymer (bearing both H-acceptor and H-donor moieties) with carbazole monomers to construct (H-acceptor only) fluorescent side-chain polymers presenting pendent pyridyl H-acceptors at various copolymeric molar ratios (100, 60, and 30 mol%) with lateral Me and MeO substituents groups. As indicated in Fig. 1, we have generated supramolecular assemblies of H-bonded nanocomposites through the interactions of the carboxylic acid surfactants (proton donors) of the surface-modified **AuSCOOH** NPs and the pyridyl groups (proton acceptors) of laterally MeO- and Me-substituted polymers (**PBTO1–PBOT3** and **PBT1–PBT3**, respectively). The fluorescent side-chain polymers **PBOT1–PBOT3** and **PBT1–PBT3** exhibited various electron-donating capabilities, thereby inducing different proton acceptor effects when titrated with the surface-functionalized Au NPs **AuSCOOH** and **AuSC10** (presenting acid and acid-free surfactants, respectively); therefore, the side-chain conjugated polymers **PBOT1–PBOT3** and **PBT1–PBT3** bearing fluorescent pyridyl H-acceptor pendent units not only behave as highly selective chemosensors for acid-functionalized Au NPs but also exhibit distinct fluorescent quenching effects upon the addition of surface-functionalized Au NPs (i.e., **AuSCOOH** and **AuSC10**, presenting acid and acid-free surfactants, respectively).

We used this approach to develop fittable exponential equations to predict the Stern–Volmer (SV) quenching constants for a diverse range of fluorescent copolymers (containing various molar ratios of pyridyl H-acceptors and different lateral functional groups) when titrated with different NP quenchers. Finally, the results of the PL titrations of the SV quenching constants suggested the optimum quenching mechanism between the fluorescent copolymers and the NPs, which may facilitate the selection of the best operating conditions (with the largest quenching effect) for the preparation of nanocomposites for the first recognition stage, with recovery of the fluorescence of the chromophores (with the strongest re-emitting effect) upon re-coordination (or re-complexation) of metal ions (or biomolecules) with the fluorophores in the second sensing stage.

2. Experimental section

2.1. Materials

Chemicals and solvents were reagent grades and purchased from Aldrich, ACROS, TCI, and Lancaster Chemical Co. Dichloromathane and THF were distilled to keep anhydrous before use. The other chemicals were used without further purification. The synthetic routes of proton acceptor polymers **PBOT1–PBOT3** and **PBT1–PBT3** (as shown in Fig. 2) were reported in our previous results [54,55]. The chemical structures of all products were confirmed by ^{1}H NMR spectroscopy and elemental analyses.

2.2. Synthesis of surface-functionalized gold nanoparticles AuSC10 and AuSCOOH

The surface-functionalized gold nanoparticles (**AuSC10** bearing acid-free surfactants) used in this study were prepared through standard Brust–Schiffrin methodology [57]. Hydrogen tetrachloroaurate aqueous solution (30 mL, 30 mmol) was mixed with tetraoctylammonium bromide (TOAB) in toluene solution (80 mL, 50 mmol). The two-phase mixture was vigorously stirred until all tetrachloroaurate was transferred into the organic layer, and then dodecanethiol (20 μL) was added to the organic phase. A freshly prepared aqueous solution of sodium borohydride (25 ml, 0.4 mol) was slowly added with vigorous stirring. After further stirring for 3 h, the organic phase was separated, and the standard Brust reaction mixture was evaporated without removing TOAB and dried completely under reduced pressure. The black solid obtained was heat-treated at 165 °C at a heating rate of 2 °C/min and

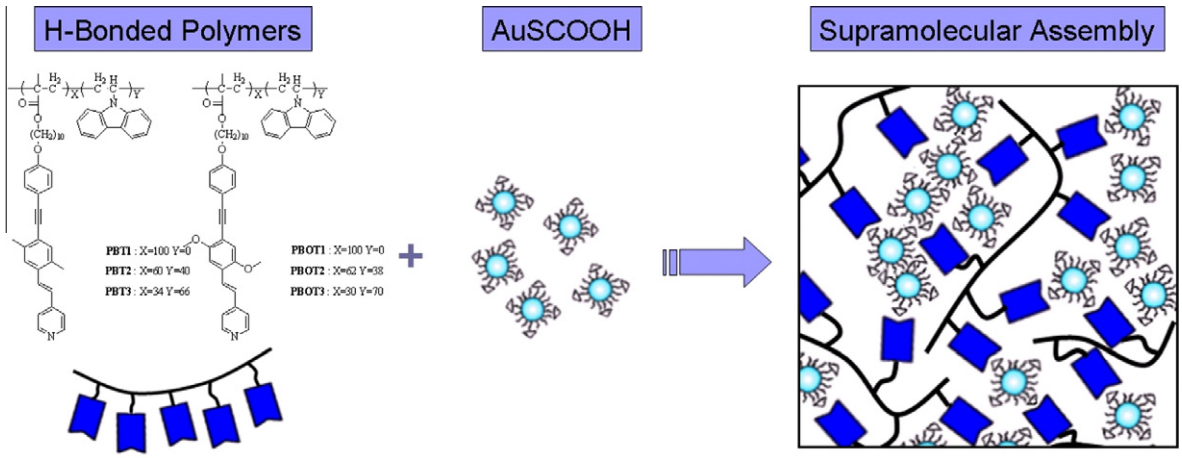

Fig. 1. Schematic illustration of fluorescent H-acceptor side-chain polymers **PBT1–PBT3** and **PBOT1–PBOT3** (with laterally methyl- and methoxy-substituted groups, respectively) complexed with acid-modified **AuSCOOH** nanoparticles.

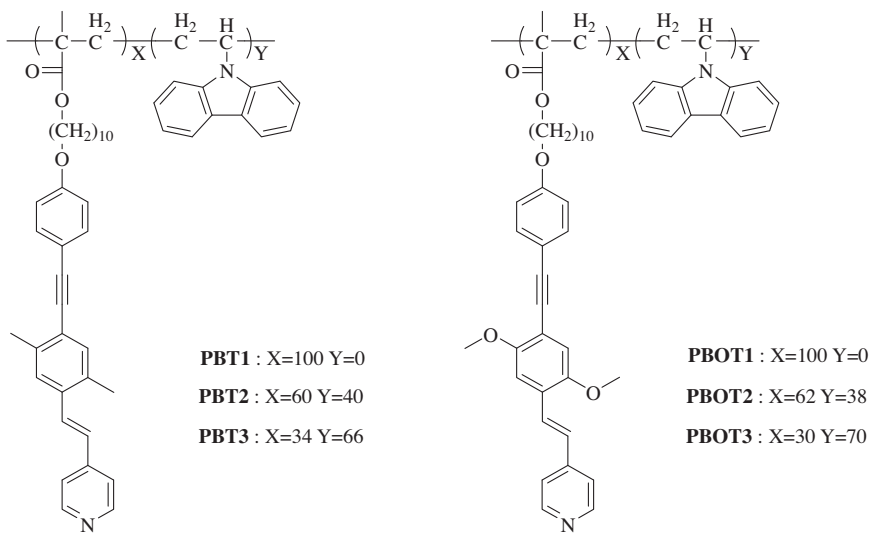

Fig. 2. Molecular structures of fluorescent H-acceptor side-chain polymers **PBT1–PBT3** and **PBOT1–PBOT3**.

held at this temperature for 30 min [58]. The thermally 'ripened' product was dissolved in toluene and washed with methanol to remove excess thiol ligands and TOAB, then **AuSC10** nanoparticles with alkyl surfactants were obtained. In the subsequent Murray place exchange reaction [59], **AuSC10** nanoparticles (60 mg) were combined with the proper amount of 11-mercaptoundecanoic acid in dichloromethane (3 mg of **AuSC10**/mL) and reacted for 48 h. After the exchange reaction was completed, the reaction mixture was concentrated using a rotary evaporator. After washing these products with a large amount of ethanol and acetone, no further purifications were conducted on these samples. Then, the acid-functionalized gold nanoparticles (**AuSCOOH**) with a diameter ca. 5–6 nm were obtained, and the monolayer compositions of **AuSCOOH** nanoparticles with both acid and alkyl surfactants were characterized by ^{1}H NMR featured 79% decanethiol and 21% carboxylic acid thiol functionalities[60–62]. In our studies of nanocomposites, both THF-soluble gold nanoparticles, i.e., alkyl-functionalized gold nanoparticles (**AuSC10** bearing acid-free surfactants) and acid-functionalized gold nanoparticles (**AuSCOOH** bearing acid surfactants), were used.

2.3. Preparation of nanocomposites consisting of gold nanoparticles and polymers

Nanocomposites were prepared by mixing solutions (0.5 mg/ml) of H-acceptor polymers **PBOT1–PBOT3** and **PBT1–PBT3** in THF (2 mg/ml) with surface-functionalized gold nanoparticles **AuSCOOH** and **AuSC10**, which contain acid and acid-free surfactants, respectively. The gold nanoparticles began to assemble into nanocomposites within 2 min. The mixed solutions became visibly turbid,

indicating that an aggregation process had occurred. After 24 h, the solid precipitates were collected and washed extensively with hexane. The nanocomposites were then dried overnight before being subjected to transmission electron microscopy (TEM) measurements.

2.4. Measurements and characterization

^{1}H NMR spectra were recorded on a Varian unity 300 M Hz spectrometer using $CDCl_3$, DMSO-d_6, *d*-dioxane, and d-THF as solvents. UV–visible absorption spectra were recorded in dilute THF solutions (10^{-6} M) on a HP G1103A spectrophotometer, and photoluminescence (PL) spectra were obtained on a Hitachi F-4500 spectrophotometer. Fourier transform infrared (FT-IR) spectra were proceeded on a Nicolet 360 FT-IR spectrometer. Transmission electron microscopy (TEM) analyses were performed using a JEOL 2011 electron microscope with an acceleration voltage of 200 keV. The samples were prepared from THF solutions with a concentration of 1 wt.%, and the aggregates were precipitated on TEM sample grids (200 Cu mesh/carbon films).

3. Results and discussion

3.1. Fourier transform infrared (FTIR) spectroscopy

We used FTIR spectroscopy to confirm the presence of hydrogen bonds in two series of supramolecular nanocomposites comprising the side-chain polymers **PBOT1**–**PBOT3** and **PBT1**–**PBT3** complexed with the acid-modified **AuSCOOH** NPs. Figure S1 (Supplementary Information) provides representative FTIR spectra of the acid-modified **AuSCOOH** NPs, the H-acceptor polymer **PBOT1**, and the H-bonded nanocomposite **PBOT1**/**AuSCOOH**. Relative to the spectrum of the acid-modified **AuSCOOH** NPs, the signal for the O–H bonds in the spectrum of the H-bonded nanocomposite **PBOT1**/**AuSCOOH** should be weaker as a result of hydrogen bonding between the pyridyl groups of **PBOT1** and the carboxylic acid units on the surface of the **AuSCOOH** NPs in the H-bonded nanocomposite. Because the content of carboxylic acid-modified surfactants was only 21% on the acid-modified **AuSCOOH** NPs, however, the O–H band of the acid-modified **AuSCOOH** NPs was too weak to be observed. On the other hand, the C═O stretching vibration at 1695 cm^{-1} for the H-bonded nanocomposite **PBOT1**/**AuSCOOH** revealed that the C═O groups were in a less-associated state than that in the acid-modified **AuSCOOH** NPs, with a weaker C═O stretching vibration at 1660 cm^{-1}, suggesting the existence of H-bonds between the polymer and the NPs. Other supramolecular polymers have exhibited similar spectroscopic behavior as a result of H-bonding in their H-bonded polymer complexes [53–55].

3.2. Fluorescence quenching of copolymers induced by surface-modified Au NPs

Fig. 3 displays the results of fluorescence quenching studies of two fluorescent side-chain homopolymers **PBOT1** and **PBT1** with lateral MeO and Me substituents, respectively, titrated with the surface-modified NPs **AuSCOOH** and **AuSC10** (average diameter: ca. 5–6 nm) at various concentrations in THF. In a previous study [55], we found that the fluorescence spectrum of the polymer **PBT1** in THF featured a signal for the emission of blue light at 440 nm. Relative to the polymer **PBT1**, the luminescent polymer **PBOT1** exhibited a red-shifted PL emission at 449 nm, due to the stronger electron donating effect of its lateral MeO groups, which induced a narrower energy band gap. In Fig. 3a and b, the H-acceptor polymers **PBOT1** and **PBT1** exhibited dramatic decreases in their fluorescence intensities upon the addition of the **AuSCOOH** NPs (containing 21% carboxylic acid surfactants). It is conceivable that the fluorescence emission intensities of the nanocomposites **PBOT1**/**AuSCOOH** and **PBT1**/**AuSCOOH** decreased as a result of the H-bonded complexation of the H-acceptor pyridyl pendent units of the fluorescent polymers (**PBOT1** and **PBT1**) with the H-donor acidic units of the surfactants on the **AuSCOOH** NPs (illustrated schematically in Fig. 1). In Fig. 3a, the fluorescent H-acceptor polymer **PBOT1** (with lateral MeO substituents) appeared to readily undergo H-bonding with the **AuSCOOH** NPs (via the carboxylic acid-modified surfactants), thereby undergoing quenching due to supramolecular interactions. For the same reason, the titration of the fluorescent H-acceptor polymer **PBT1** (with lateral Me substituents) with the **AuSCOOH** NPs (Fig. 3b) revealed similar PL quenching. These results suggest that the complexation of **PBT1** with the **AuSCOOH** NPs featured H-bonding interactions similar to those in the nanocomposite **PBOT1**/**AuSCOOH**, as confirmed in our TEM analyses (see below). For comparison, we titrated the fluorescent polymers **PBOT1** and **PBT1** with the alkyl-functionalized Au NPs **AuSC10**, presenting acid-free surfactant units. Again, we observed similar decreases in PL for the fluorescent polymers **PBOT1** and **PBT1** upon the addition of the **AuSC10** NPs (Fig. 3c and d). In progressive fluorescence quenching experiments of the polymers **PBOT1** and **PBT1** upon increasing the concentration of **AuSC10**, in contrast to H-bonded nanocomposites (i.e., **PBOT1**/**AuSCOOH** and **PBT1**/**AuSCOOH**) we detected much weaker quenching behavior of the nanocomposites **PBOT1**/**AuSC10** and **PBT1**/**AuSC10**. Because of the lack of H-bonding interactions of the **AuSC10** NPs (containing the acid-free surfactant units) with the fluorescent polymers **PBOT1** and **PBT1**, these NPs had much weaker PL quenching effects on **PBOT1** and **PBT1** than did the acid-modified **AuSCOOH** NPs.

Comparing the curves in the insets to Fig. 3a–d, the fluorescence quenching patterns for the polymers **PBOT1** and **PBT1** titrated with **AuSCOOH** (Fig. 3a and b) were much stronger than those titrated by **AuSC10** (Fig. 3c and d). Therefore, the distinct quenching effects during the PL titrations of the fluorescent polymers **PBOT1** and **PBT1** by the different surface-modified **AuSCOOH** and **AuSC10** NPs confirmed the presence of H-bonding interactions in the nanocomposites **PBOT1**/**AuSCOOH** and **PBT1**/**AuSCOOH**. In addition, upon addition of the surface-modified **AuSCOOH** and **AuSC10** NPs, we observed analogous fluorescence quenching tendencies (albeit to different degrees) in the PL spectra in Figures S2 and S3 (Supplementary

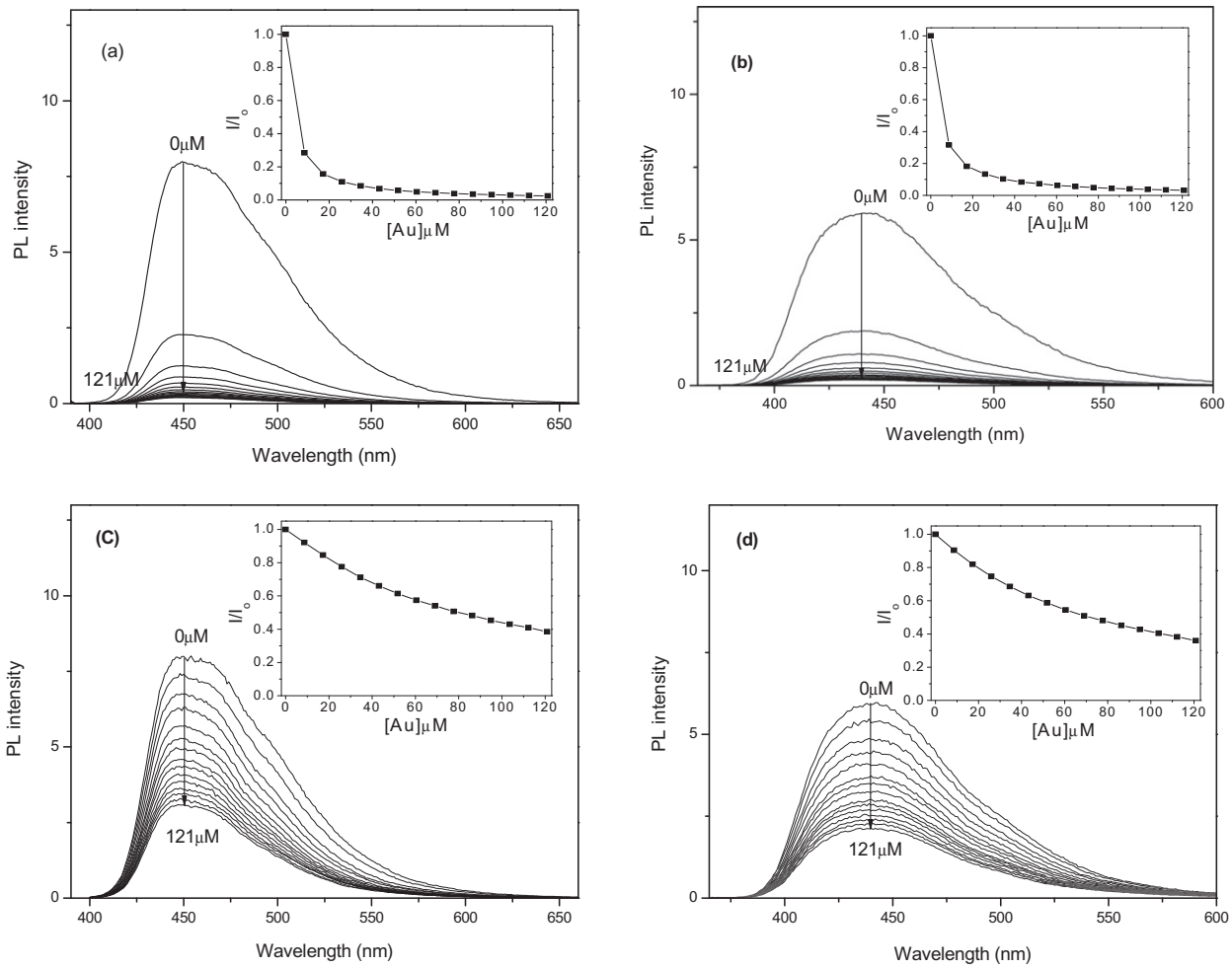

Fig. 3. Fluorescence quenching spectra of fluorescent homopolymers **PBOT1** and **PBT1** titrated with different nanoparticle quenchers (**AuSCOOH** and **AuSC10**) in THF solutions: (a) **PBOT1** and (b) **PBT1** by varying the concentration of acid-donor-modified **AuSCOOH** nanoparticles; (c) **PBOT1** and (d) **PBT1** by varying the concentration of non-acid-modified **AuSC10** nanoparticles.

Information) for the fluorescent copolymers **PBOT2–PBOT3** and **PBT2–PBT3** (bearing various molar ratios of pyridyl groups). Nonetheless, although these nanocomposites exhibited comparable PL quenching trends, the various Stern–Volmer (SV) quenching constants (K_{SV}) for the diverse fluorescent polymers **PBOT1–PBOT3** and **PBT1–PBT3** (containing various molar ratios of pyridyl H-acceptors with lateral MeO and Me substituents) could be predicted specifically upon titration with the different NP quenchers (i.e., the surface-modified NPs **AuSCOOH** and **AuSC10**) in the following investigations of the PL quenching behavior. Hence, more comprehensible quenching details can be explored by the following investigation. Normally, the PL quenching behavior follows the SV relationship [56]:

$$I_0/I = 1 + K_{SV}[Q]$$

where I_0 and I are the emission intensities of the fluorescent polymer (in this case, **PBOT1–PBOT3** or **PBT1–PBT3**) in the absence and presence, respectively, of the quencher Q (here, surface-modified Au NPs); K_{SV} is the SV quenching constant; and [Q] is the concentration of the quencher. Fig. 4 presents the SV plots of the polymers **PBOT1–PBOT3** and **PBT1–PBT3** in the presence of various concentrations of the carboxylic acid-modified **AuSCOOH** NPs and the non-acid-modified **AuSC10** NPs; these data were replotted from the insets to Fig. 3a–d. We obtained the quenching constants (K_{SV}) of the fluorescent polymers **PBOT1–PBOT3** and **PBT1–PBT3**, when titrated with the different NP quenchers (**AuSCOOH** and **AuSC10**) in THF, from the slopes of the plots in Fig. 4 (along with the inset slopes); Table 1 summarizes these values. Interestingly, comparing the fluorescence quenching effects of the **AuSCOOH** NPs on the homopolymers **PBOT1** and **PBT1**, we find that the quenching constant of **PBOT1** (lateral MeO substituents; $K_{SV} = 3.31 \times 10^5\ M^{-1}$) was higher than that of **PBT1** (lateral Me substituents; $K_{SV} = 2.50 \times 10^5\ M^{-1}$). We suspect that, due to the more strongly electron-donating MeO groups of the conjugated pendent units of **PBOT1**, the pyridyl units of **PBOT1** exerted a greater proton acceptor effect

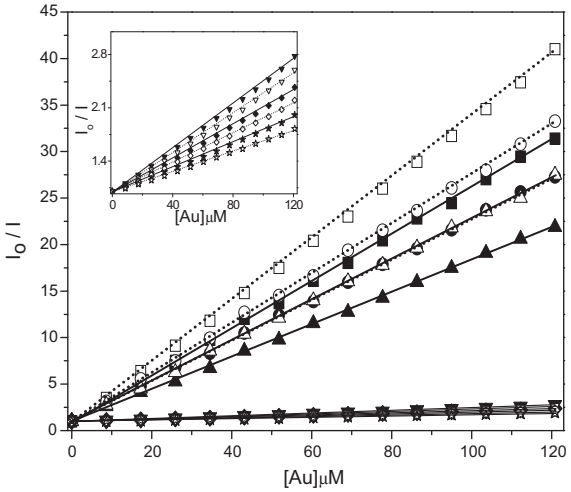

Fig. 4. Corresponding Stern–Volmer plots of polymers **PBOT1** (□), **PBOT2** (○), **PBOT3** (△), **PBT1** (■), **PBT2** (●), and **PBT3** (▲) for various concentrations of acid-modified **AuSCOOH** nanoparticles as well as polymers **PBOT1** (▽), **PBOT2** (◇), **PBOT3** (☆) **PBT1** (▼), **PBT2** (◆), and **PBT3** (★) for various concentrations of non-acid-modified **AuSC10** nanoparticles in THF solutions, where polymers **PBOT1-PBOT3** and **PBT1-PBT3** for various concentrations of non-acid-modified **AuSC10** nanoparticles are replotted in the inset.

than did those of the pyridyl units in **PBT1** upon complexation with **AuSCOOH**. Therefore, the strongest H-bonding interaction—that of **AuSCOOH** with **PBOT1** in the nanocomposite **PBOT1**/**AuSCOOH**—induced the largest quenching constant in the PL titration experiments. Similarly, when titrated with the acid-modified **AuSCOOH** NPs, the copolymers **PBOT2** and **PBOT3** with lateral MeO substituents (but different molar ratios of pyridyl groups) also exhibited larger quenching constants ($K_{SV} = 2.67 \times 10^5$ and 2.19×10^5 M^{-1}, respectively) than did the copolymers **PBT2** and **PBT3** with lateral Me substituents ($K_{SV} = 2.17 \times 10^5$ and 1.7×10^5 M^{-1}, respectively). The lower quenching constants of the fluorescent copolymers **PBOT2** and **PBOT3** and of **PBT2** and **PBT3** relative to those of the homopolymers **PBOT1** and **PBT1** (when titrated with **AuSCOOH**) might be due to their lower molar ratios of pyridyl H-acceptors, thereby affecting the homogenous dispersion of the **AuSCOOH** NPs and minimizing their PL quenching effects.

On the other hand, because of the absence of H-bonding interactions when we titrated the homopolymers **PBOT1** and **PBT1** with the non-acid-modified **AuSC10** NPs (inset to Fig. 4), the quenching constants of **PBOT1** and **PBT1** ($K_{SV} = 2.15 \times 10^4$ and 2.30×10^4 M^{-1}, respectively) were both much lower than those ($K_{SV} = 3.31 \times 10^5$ and 2.50×10^5 M^{-1}, respectively) obtained when titrated with the carboxylic acid-modified **AuSCOOH** NPs (forming H-bonded nanocomposites). Surprisingly, when titrated with the non-acid-modified **AuSC10** NPs, the quenching constant ($K_{SV} = 2.15 \times 10^4$ M^{-1}) of **PBOT1** was less than that ($K_{SV} = 2.30 \times 10^4$ M^{-1}) of **PBT1**. Hence, the quenching mechanisms of **PBOT1** and **PBT1** induced by the non-acid-modified **AuSC10** NPs (in the absence of H-bonds) are different from those induced by the acid-modified **AuSCOOH** NPs (in the presence of H-bonds). Here, the assembly of the fluorescent polymers **PBOT1** and **PBT1** with the non-acid-modified **AuSC10** NPs originated from dipole–dipole interactions, rather than H-bonding. Consequently, the dipole–dipole interactions of the **AuSC10** NPs with **PBOT1** (lateral MeO groups) were stronger than those with **PBT1** (lateral Me groups). As a result, the stronger binding interactions of the **AuSC10** NPs with **PBOT1** (lateral MeO groups) induced less quenching because of the weaker association of the pyridyl conjugated structures in **PBOT1** with the **AuSC10** NPs. Overall, the lateral MeO groups competed with the pyridyl termini of the polymer **PBOT1** for interactions with the non-acid-modified **AuSC10** NPs, thereby diluting the quenching effects of the **AuSC10** NPs toward the polymer **PBOT1** and, as a result, decreasing its value of K_{SV}. Accordingly, when titrated with the non-acid-modified **AuSC10** NPs (inset to Fig. 4), the copolymers **PBOT2** and **PBOT3** with lateral MeO substituents (but with different molar ratios of pyridyl groups) also exhibited smaller quenching constants ($K_{SV} = 1.82 \times 10^5$ and 1.51×10^5 M^{-1}, respectively) relative to those of the copolymers **PBT2** and **PBT3** with lateral Me substituents ($K_{SV} = 1.96 \times 10^5$ and 1.66×10^5 M^{-1}, respectively). We suspect that the smaller quenching constants of the fluorescent copolymers **PBOT2**, **PBOT3**, **PBT2**, and **PBT3** relative to those of the homopolymers **PBOT1** and **PBT1** (when titrated with **AuSC10**) resulted from the lower molar ratios of pyridyl H-acceptors in the former copolymers (and weaker dipole–dipole interactions with the NPs), thereby minimizing the aggregation of the **AuSC10** NPs and decreasing their PL quenching effects.

Because of the absence of H-bonding interactions in the nanocomposites **PBOT1–PBOT3/AuSC10** and **PBT1–PBT3/AuSC10**, all of the values of K_{SV} (in Table 1) of the polymers **PBOT1–PBOT3** and **PBT1–PBT3** blended with the non-acid-modified Au NPs (**AuSC10**) were much (ca. 10 times) lower than those obtained when H-bonded with the

Table 1
Stern–Volmer constants (*K*sv) for polymers **PBOT1–PBOT3** and **PBT1–PBT3** titrated with different nanoparticle quenchers (AuSCOOH and AuSC10) in THF solutions.

	K_{SV} (M^{-1})[a]					
	PBT1	PBT2	PBT3	PBOT1	PBOT2	PBOT3
AuSCOOH	2.50×10^5	2.17×10^5	1.70×10^5	3.31×10^5	2.67×10^5	2.19×10^5
AuSC10	2.30×10^4	1.96×10^4	1.66×10^4	2.15×10^4	1.82×10^4	1.51×10^4

[a] The quenching behavior follows the Stern–Volmer relation $I_0/I = 1 + K_{SV}[Q]$, where I_0 and I are the emission intensities of the fluorescent polymers (**PBOT1–PBOT3** and **PBT1–PBT3**) in the absence and presence of the nanoparticle quencher Q (surface-functionalized gold nanoparticles **AuSCOOH** and **AuSC10**), respectively, K_{SV} is the Stern–Volmer quenching constant, and [Q] is the concentration of the nanoparticle quencher.

carboxylic acid-modified Au NPs (**AuSCOOH**). Hence, H-bonding interactions played a very important role in determining the PL quenching effect of the fluorescent polymers induced by the Au NPs. Moreover, we have developed a multicomponent self-assembly process involving PL quenching of fluorescent polymers (such as polymers **PBOT1**–**PBOT3** and **PBT1**–**PBT3** with various molar ratios of pyridyl H-acceptors) titrated by different surface-modified Au NPs (**AuSCOOH** and **AuSC10** bearing acid and acid-free surfactants, respectively), which can be utilized by other systems in the future study. On the whole, significant supramolecular interactions between various surface-modified Au NPs and fluorescent polymers can be distinguished merely by the distinct fluorescence quenching behavior with specific quenching constants (K_{SV}). Interestingly, as the molar ratio of the pyridyl units in the fluorescent polymers decreased, the values of K_{SV} decreased exponentially (Fig. 5), suggesting that the plots of the SV constants followed the fittable exponential equation:

$$K_{SV} = A(1 - e^{-BX})$$

where X is the mole percentage of pyridyl units in the fluorescent polymers and A and B are constants for the exponential curve fittings. Fig. 5 displays the fitted exponential curves and data points (acquired from the slopes of the SV plots in Fig. 4 and Table 1) of the SV constants (K_{SV}) for the nanocomposites **PBOT/AuSCOOH** ($A = 3.33 \times 10^5$, $B = 3.21$), **PBT/AuSCOOH** ($A = 2.61 \times 10^5$, $B = 3.06$), **PBT/AuSC10** ($A = 2.33 \times 10^4$, $B = 3.47$), and **PBOT/AuSC10** ($A = 2.13 \times 10^4$, $B = 3.78$). Using this plot, it would be easy to predict the SV constants of fluorescent polymers containing other molar ratios of pyridyl conjugated units. Compared with the H-bonded nanocomposites **PBOT**/**AuSCOOH** and **PBT**/**AuSCOOH**, the much lower values of K_{SV} of the polymers **PBOT1**–**PBOT3** and **PBT1**–

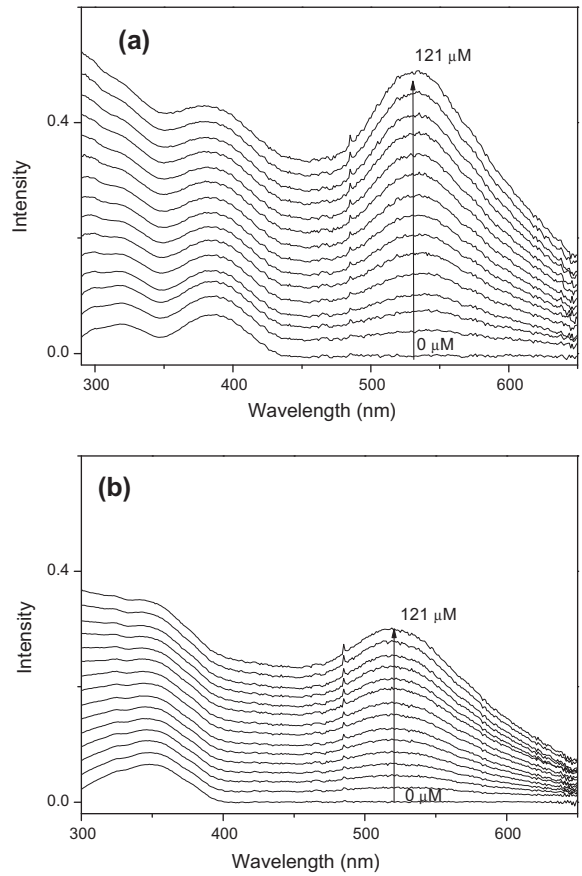

Fig. 6. UV–visible spectra of (a) polymer **PBOT1** titrated by varying the concentration of acid-donor-modified gold nanoparticles **(AuSCOOH**) and (b) polymer **PBT1** titrated by varying the concentration of non-acid-modified gold nanoparticles (**AuSC10)** in THF solutions.

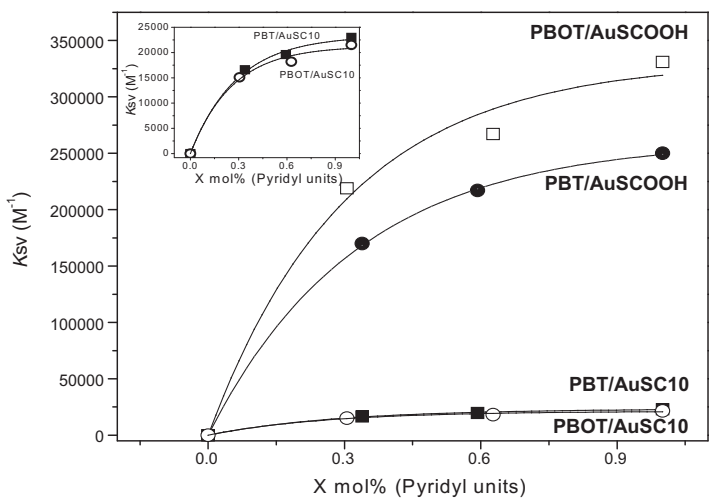

Fig. 5. Schematic curves of Stern–Volmer constants (Ksv) vs. mol% of pyridyl units (X) in fluorescent polymers **(PBOT1-PBOT3** and **PBT1-PBT3**) as titrated by different nanoparticle quenchers (**AuSCOOH** and **AuSC10**), which follow the exponential equation (as lines) of Ksv = A[1 − exp(−BX)], where A and B are constants for the exponential curve fittings. The data points of Stern–Volmer constants (Ksv) for nanocomposites **PBOT/AuSCOOH** (□), **PBT/AuSCOOH** (●), **PBT/AuSC10** (■), and **PBOT/AuSC10** (○) were acquired from the slopes of Stern–Volmer plots in Fig. 4 and Table 1, and their (A and B) values for the exponential curve fittings are ($A = 3.33 \times 10^5$, $B = 3.21$), ($A = 2.61 \times 10^5$, $B = 3.06$), ($A = 2.33 \times 10^4$, $B = 3.47$), ($A = 2.13 \times 10^4$, $B = 3.78$), respectively.

PBT3, respectively, when blended with the non-acid-modified **AuSC10** NPs (without H-bonding), necessitated that we enlarged the exponential curves of the values of K_{SV} for the nanocomposites **PBOT**/**AuSC10** and **PBT**/**AuSC10** when plotted in the inset to Fig. 5.

To confirm the fluorescence quenching effects induced by the surface-modified Au NPs **AuSCOOH** and **AuSC10** on the fluorescent polymers **PBOT1**–**PBOT3** and **PBT1**–**PBT3**, we recorded the UV–Vis absorption spectra of polymer nanocomposites containing **AuSCOOH** and **AuSC10** [Fig. 6 and S4 and S5 (Supplementary Information)]. We would expect the UV–Vis absorption signals to change if the aggregation of fluorescent polymers was induced upon the addition of surface-modified Au NPs; here, we used the same processing conditions as those we had used for the quenching titrations of the fluorescent polymers with the Au NPs. The absorption maxima of the polymers **PBOT1** (384 nm in THF) and **PBT1** (350 nm in THF) in Fig. 6a and b, titrated with **AuSCOOH** and **AuSC10**, respectively, were not red-shifted upon increasing the concentrations of the Au NPs (from 0 to 121 μM). Here, we employed relatively low concentrations (<121 μM) of the Au NPs to avoid aggregation of the fluorescent polymers and the Au NPs during the titration process; as a result, we could exclude the effects of fluorescence quenching, due to aggregation of the fluorescent polymers, upon the addition of the Au NPs. Therefore, we can attribute the fluorescence quenching as arising mainly from energy transfer from the fluorescent polymers to the Au NPs.

3.3. TEM analyses

To confirm the source of the fluorescence quenching effects on the fluorescent polymers **PBOT1**–**PBOT3** and **PBT1**–**PBT3** induced by the surface-modified Au NPs (**AuSCOOH** and **AuSC10**), we recorded TEM images of their polymer nanocomposites [Fig. 7 and S6 (Supplementary Information)]. These images provided further insight into the morphologies of the NP aggregates. As revealed in Fig. 7a, the carboxylic acid-functionalized Au NPs (**AuSCOOH**) having an average diameter of approximately 5–6 nm aggregated strongly because of the self-assembly of their H-bonded surfactant units. Next, we drop-casted (onto TEM grids) solutions of the polymer nanocomposites prepared from the polymers **PBOT1**–**PBOT3** and **PBT1**–**PBT3** (2 mg/mL) blended with the surface-modified Au NPs **AuSCOOH** and **AuSC10** (0.5 mg/mL) in THF. The structural ensembles revealed in the TEM images of these polymer nanocomposites were controlled by both H-bonding and dipole–dipole interactions. The H-bonding interactions in the polymer nanocomposites **PBOT1**/**AuSCOOH** and **PBT1**/**AuSCOOH** involved the carboxylic acid units on the surface-functionalized **AuSCOOH** NPs coordinating with the pyridyl groups on the homopolymers **PBTO1** and **PBT1**. Thus, as revealed in Fig. 7b and **c**, addition of the carboxylic acid-modified **AuSCOOH** NPs to the polymers **PBTO1** and **PBT1** resulted in homogeneous distributions of the **AuSCOOH** NPs among the polymers, induced by the H-bonded structures in these nanocomposites. In addition, because of weaker

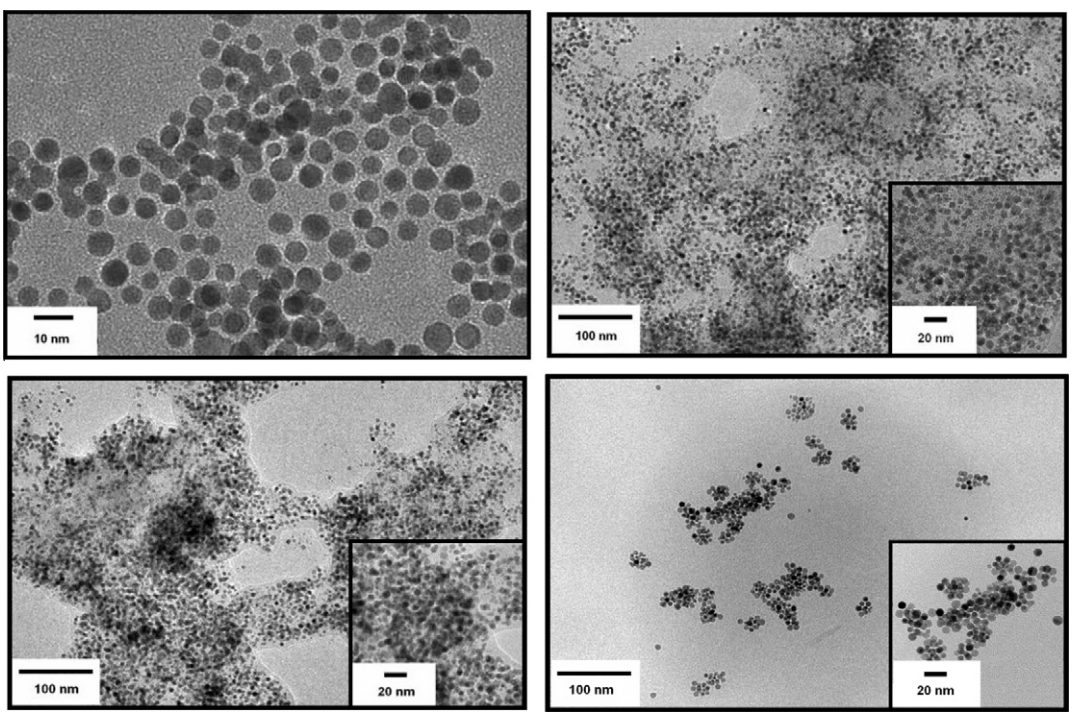

Fig. 7. TEM images of surface-modified gold nanoparticles and polymer nanocomposite (a) acid-modified **AuSCOOH** nanoparticles, (b) nanocomposite **PBOT1/AuSCOOH**, (c) nanocomposite **PBT1/AuSCOOH**, and (d) nanocomposite **PBT1/AuSC10.**

supramolecular interactions, the **AuSCOOH** NPs were dispersed only partially in the copolymers **PBOT2**, **PBOT3**, **PBT2**, and **PBT3** (because of their lower molar contents of pyridyl moieties), as revealed in their respective TEM images [see Figure S6 (Supplementary Information)]. To distinguish the contributions from the acid and acid-free surfactants on the surface-modified NPs **AuSCOOH** and **AuSC10**, respectively, we also blended the polymer **PBT1** with the non-acid-modified **AuSC10** NPs (i.e., in the absence of H-bonds). Fig. 7**d** reveals clearly that the non-acid-modified **AuSC10** NPs aggregated more extensively within polymer **PBT1**, suggesting the absence of H-bonding interactions in the nanocomposite **PBT1**/**AuSC10**. Thus, the TEM images provided evidence to explain the PL quenching behavior in the polymer nanocomposites, where a better distribution of NPs among the polymers, due to H-bonds, would result in stronger PL quenching effects on the fluorescent polymers induced by suitably surface-modified Au NPs.

4. Conclusion

We have employed two series of fluorescent side-chain polymers, **PBOT1**–**PBOT3** and **PBT1**–**PBT3** with lateral MeO and Me substituents, respectively, but different molar ratios of their pyridyl H-acceptor moieties, and surface-modified Au NPs bearing acid and acid-free surfactants (**AuSCOOH** and **AuSC10**, respectively) to develop distinct nanocomposites. The H-acceptor polymers **PBOT1**–**PBOT3** and **PBT1**–**PBT3** were quenched by the surface-modified NPs **AuSCOOH** and **AuSC10** to different extents depending on the degrees of H-bonding and dipole–dipole interactions among the fluorescent polymers and surface-modified NPs. In contrast to the predominant dipole–dipole interactions of the nanocomposites containing the non-acid-modified **AuSC10** NPs, the stronger supramolecular interactions (H-bonds) in the self-assembled nanocomposites **PBOT1**–**PBOT3/AuSCOOH** and **PBT1**–**PBT3/AuSCOOH** facilitated the dispersion of the carboxylic acid-modified **AuSCOOH** NPs among the H-acceptor polymers, thereby providing larger fluorescence quenching effects. Due to the strong electron-donating ability of the MeO substituents in the conjugated pendent units of **PBOT1**, the pyridyl units in **PBOT1** exerted a stronger proton acceptor effect relative to that of the pyridyl units in **PBT1** upon complexation with the **AuSCOOH** NPs. Therefore, upon addition of the **AuSCOOH** NPs, the quenching constant of the laterally MeO-substituted polymer **PBOT1** was greater than that of the laterally Me-substituted polymer **PBT1**. After titrating with various surface-modified NPs, we measured the PL quenching constants and behaviors of the fluorescent polymers and established an exponential equation to predict the SV constants of fluorescent polymers with other molar ratios of pyridyl conjugated units. Moreover, TEM images confirmed that the dispersion of the surface-functionalized Au NPs followed the supramolecular assembly behavior of the nanocomposites between the fluorescent polymers and the surface-functionalized Au NPs that we had observed in the PL quenching experiments. Based on the fluorescence quenching and recovery of such Au nanocomposites, we believe that the ability to develop chemosensor and biosensor applications will be available in the near future.

Acknowledgements

The TEM measurements are supported by Institute of Chemistry, Academia Sinica (Taiwan). The financial support provided by the National Science Council of Taiwan (ROC) through NSC 97-2113-M-009-006-MY2 and Chung-Shan Institute of Science and Technology (Taiwan) are acknowledged for this project.

Appendix A. Supplementary data

Supplementary data associated with this article can be found, in the online version, at doi:10.1016/j.eurpolymj.2011.09.024.

References

[1] Vriezema DM, Aragonés MC, Elemans JAAW, Cornelissen JJLM, Rowan AE, Nolte RJM. Self-assembled nanoreactors. Chem Rev 2005;105(4):1445–90.
[2] Pollino JM, Weck M. Non-covalent side-chain polymers: design principles, functionalization strategies, and perspectives. Chem Soc Rev 2005;34:193–207.
[3] Burd C, Weck MJ. Solvent influence on the orthogonality of noncovalently functionalized terpolymers. J Polym Sci Part A Polym Chem 2008;46:1936–44.
[4] Tang C, Lennon EM, Fredrickson GH, Kramer EJ, Hawker CJ. Evolution of block copolymer lithography to highly ordered square arrays. Science 2008;322:429–32.
[5] Didehban K, Namazi H, Entezami AA. Non-covalent dendrimer-based liquid crystalline complexes: synthesis and characterization. Eur Polym J 2010;46(9):1923–31.
[6] Liang TC, Chiang IH, Yang PJ, Kekuda D, Chu CW, Lin HC. Supramolecular assembly of H-bonded side-chain polymers containing conjugated pyridyl H-acceptor pendants and various low-band-gap H-donor dyes bearing cyanoacrylic acid groups for organic solar cell applications. J Polym Sci Part A Polym Chem 2009;47:5998–6013.
[7] Wang LY, Chiang IH, Yang PJ, Li WS, Chao IT, Lin HC. Configuration effects of H-bonded sites and rigid core lengths on H-bonded banana-shaped liquid crystalline supramolecules consisting of symmetric trimers and asymmetric heterodimers. J Phys Chem B 2009;113:14648–60.
[8] Moughton AO, Stubenrauch K, O'Reilly RK. Hollow nanostructures from self-assembled supramolecular metallo-triblock copolymers. Soft Matter 2009;5:2361–70.
[9] O'Reilly RK, Joralemon MJ, Hawker CJ, Wooley KL. Facile syntheses of surface-functionalized micelles and shell cross-linked nanoparticles. J Polym Sci Part A Polym Chem 2006;44:5203–17.
[10] Winter A, Friebe C, Chiper M, Hager MD, Schubert US. Self-assembly of π-conjugated bis(terpyridine) ligands with zinc(II) ions: new metallosupramolecular materials for optoelectronic applications. J Polym Sci Part A Polym Chem 2009;47:4083–98.
[11] Noormofidi N, Slugovc C. Optical response of phenantroimidazole–dyes covalently linked to a polynorbornene-backbone to acid and base. Euro Polym Jnl 2010;46(4):694–701.
[12] Gibson HW, Farcas A, Jones JW, Ge ZX, Huang FH, Vergne M, et al. Supramacromolecular self-assembly: chain extension, star and block polymers via pseudorotaxane formation from well-defined end-functionalized polymers. J Polym Sci Part A Polym Chem 2009;47:3518–43.
[13] Lin HC, Tsai CM, Huang GH, Tao YT. Synthesis and characterization of light-emitting H-bonded complexes and polymers containing bis(pyridyl) emitting acceptors. Macromolecules 2006;39:557–68.

[14] Wu CW, Lin HC. H-bonded effects on novel supramolecular dendrimers containing electron-transporting donor dendrons and single/double H-bonded acceptor emitters. Macromolecules 2006;39:7985–97.
[15] Lin HC, Jiang MD, Wu SC, Jou LL, Chou KP, Huang CM, et al. Self-assembly of H-bonded side-chain and cross-linking copolymers containing diblock-copolymeric donors and single/double H-bonded light-emitting acceptors. J Polym Sci Part A Polym Chem 2009;47: 4685–702.
[16] Boal AK, Ilhan F, DeRouchey JE, Thurn-Albrecht T, Russell TP, Rotello VM. Self-assembly of nanoparticles into structured spherical and network aggregates. Nature 2000;404:746–8.
[17] Shenhar R, Rotello VM. Nanoparticles: Scaffolds and building blocks. Acc Chem Res 2003;36:549–61.
[18] Uzun O, Frankamp BL, Sanyal A, Rotello VM. Recognition-mediated assembly of nanoparticle-diblock copolymer micelles with controlled size. Chem Mater 2006;18:5404–9.
[19] Cooke G, Garety JF, Hewage SG, Rabani G, Rotello VM, Woisel P. The tuneable complexation of gold nanoparticles. Chem Commun 2006: 4119–21.
[20] Yu X, Samanta B, Xu H, Arumugam P, Ofir Y, Jordan BJ, et al. Fabrication and functionalization of supramolecular microgel arrays through complementary hydrogen-bonding interactions. Small 2009;5:86–9.
[21] Padhy H, Sahu D, Chiang IH, Patra D, Kekuda D, Chu CW, et al. Synthesis and applications of main-chain Ru(II) metallo-polymers containing bis-terpyridyl ligands with various benzodiazole cores for solar cells. J Mater Chem 2011;21:1196–205.
[22] Chen YY, Lin HC. Synthesis and characterization of light-emitting main-chain metallo-polymers containing bis-terpyridyl ligands with various lateral substituents. J Polym Sci Part A Polym Chem 2007;45: 3243–55.
[23] Swager TM. The molecular wire approach to sensory signal amplification. Acc Chem Res 1998;31:201–7.
[24] Fan LJ, Jones Jr WE. A highly selective and sensitive inorganic/organic hybrid polymer fluorescence "Turn-on" chemosensory system for Iron cations. J Am Chem Soc 2006;128:6784–5.
[25] Martínez-Máñez R, Sancenón F. Fluorogenic and chromogenic chemosensors and reagents for anions. Chem Rev 2003;103(11): 4419–76.
[26] Luo J, Yang C, Zheng J, Ma J, Liang, Lu M. Synthesis and photophysics properties of novel bipolar copolymers containing quinoline aluminum moieties and carbazole segments. Euro Polym J 2011;47(3):385–93.
[27] Chu HC, Lee YH, Hsu SJ, Yang PJ, Yabushita A, Lin HC. Novel reversible chemosensory material based on conjugated side-chain polymer containing fluorescent pyridyl receptor pendants. J Phys Chem B 2011;115:8845–52.
[28] Thomas III SW, Joly GD, Swager TM. Chemical sensors based on amplifying fluorescent conjugated polymers. Chem Rev 2007; 107(4):1339–86.
[29] Li H, Valiyaveettil S. Water-soluble multifunctional cross-conjugated poly(*p*-phenylenes) as stimuli-responsive materials: design, synthesis, and characterization. Macromolecules 2007;40:6057–66.
[30] Carmona T, Fernández-Peña N, Tarazona MP, Saiz E, Mendicuti F. Characterization of *N*-vinyl carbazole/vinyl 4-*tert*-butyl-benzoate copolymers of several molar compositions: SEC, DSC and intramolecular excimers in dilute solutions. Euro Polym J 2010;46(8):1796–809.
[31] Zhao X, Jiang H, Schanze KS. Polymer chain length dependence of amplified fluorescence quenching in conjugated polyelectrolytes. Macromolecules 2008;41:3422–8.
[32] Yang JS, Swager TM. Fluorescent porous polymer films as TNT chemosensors: electronic and structural effects. J Am Chem Soc 1998;120:11864–73.
[33] Fan C, Plaxco KW, Heeger AJ. High-efficiency fluorescence quenching of conjugated polymers by proteins. J Am Chem Soc 2002;124: 5642–3.
[34] McCullough RD, Ewbank PC, Loewe RS. Self-assembly and disassembly of regioregular, water soluble polythiophenes: chemoselective ionchromatic sensing in water. J Am Chem Soc 1997;119:633–4.
[35] Gaylord BS, Heeger AJ, Bazan GC. DNA hybridization detection with water-soluble conjugated polymers and chromophore-labeled single-stranded DNA. J Am Chem Soc 2003;125:896–900.
[36] Kimura M, Horai T, Hanabusa K, Shirai H. Fluorescence chemosensor for metal ions using conjugated polymers. Adv Mater 1998;10:459–62.
[37] Balamurugan A, Reddy MLP, Jayakannan M. Carboxylic-functionalized water soluble π-conjugated polymer: highly selective and efficient chemosensor for mercury (II) ions. J Polym Sci Part A Polym Chem 2009;47:5144–57.
[38] Thomas KG, Kamat PV. Chromophore-functionalized gold nanoparticles. Acc Chem Res 2003;36:888–98.
[39] Bayir A, Jordan BJ, Verma A, Pollier MA, Cooke G, Rotello VM. Model systems for flavoenzyme activity: recognition and redox modulation of flavin mononucleotide in water using nanoparticles. Chem Commun 2006:4033–5.
[40] Barazzouk S, Kamat PV, Hotchandani S. Photoinduced electron transfer between Chlorophyll a and Gold nanoparticles. J Phys Chem B 2005;109(2):716–23.
[41] George WN, Giles M, McCulloch I, de Mello JC, Steinke JHG. Amplified fluorescence quenching in high ionic strength media. Soft Matter 2007;3:1381–7.
[42] Daniel MC, Astruc D. Gold nanoparticles: assembly, supramolecular chemistry, quantum-size-related properties, and applications toward biology, catalysis, and nanotechnology. Chem Rev 2004;104(1):293–346.
[43] Burda C, Chen X, Narayanan R, El-Sayed MA. Chemistry and properties of nanocrystals of different shapes. Chem Rev 2005;105(4):1025–102.
[44] Meristoudi A, Pispas S. Polymer mediated formation of corona-embedded gold nanoparticles in block polyelectrolyte micelles. Polymer 2009;50:2743–51.
[45] Ku SJ, Woo SA, Seo D, Song H, Kim JB. Simple fabrication of patterned gold nanoparticle arrays on functionalized block copolymer thin films. Euro Polym J 2011;47(3):305–10.
[46] Kumar S, Pal SK, Kumar PS, Lakshminarayanan V. Novel conducting nanocomposites: synthesis of triphenylene-covered gold nanoparticles and their insertion into a columnar matrix. Soft Matter 2007;3:896–900.
[47] Fragoso A, Sanromà B, Ortiz M, O'Sullivan CK. Layer-by-layer self-assembly of peroxidase on gold electrodes based on complementary cyclodextrin–adamantane supramolecular interactions. Soft Matter 2009;5:400–6.
[48] Cheng PPH, Silvester D, Wang G, Kalyuzhny G, Douglas A, Murray RW. Dynamic and static quenching of fluorescence by 1–4 nm diameter gold monolayer-protected clusters. J Phys Chem B 2006;110:4637–44.
[49] Ipe BI, Thomas KG, Barazzouk S, Hotchandani S, Kamat PV. Photoinduced charge separation in a fluorophore–gold nanoassembly. J Phys Chem B 2002;106:18–21.
[50] Wang Y, Liu B. Amplified fluorescence Turn-On assay for Mercury(II) detection and quantification based on conjugated polymer and silica nanoparticles. Macromol Rapid Commun 2009;30:498–503.
[51] Huang X, Xu Y, Zheng L, Meng J, Cheng Y. A highly selective and sensitive fluorescence chemosensor based on optically active polybinaphthyls for Hg^{2+}. Polymer 2009;50:5996–6000.
[52] He X, Zhong Z, Guo Y, Lv J, Xu J, Zhu M, et al. Gold nanoparticle-based monitoring of the reduction of oxidized to reduced Glutathione. Langmuir 2007;23:8815–9.
[53] Liang TC, Lin HC. Supramolecular assembly of H-bonded copolymers/complexes/nanocomposites and fluorescence quenching effects of surface-modified gold nanoparticles on fluorescent copolymers containing pyridyl H-acceptors and acid H-donors. J Mater Chem 2009;19:4753–63.
[54] Yang PJ, Wu CW, Sahu D, Lin HC. Study of supramolecular side-chain copolymers containing light-emitting H-acceptors and electron-transporting dendritic H-donors. Macromolecules 2008;41: 9692–703.
[55] Liang TC, Lin HC. Study of supramolecular side-chain and cross-linking polymers by complexation of various H-donor acids with H-acceptor copolymers containing pendent carbazole and fluorescent pyridyl units. J Polym Sci Part A Polym Chem 2009;47:2734–53.
[56] Dai Q, Worden JG, Trullinger J, Huo Q. A "Nanonecklace" synthesized from monofunctionalized gold nanoparticles. J Am Chem Soc 2005;127:8008–9.
[57] Brust M, Walker M, Bethell D, Schiffrin DJ, Whyman R. Synthesis of thiol-derivatised gold nanoparticles in a two-phase Liquid–Liquid system. J Chem Soc Chem Commun 1994:801–2.
[58] Teranishi T, Hasegawa S, Shimizu T, Miyake M. Heat-Induced size evolution of gold nanoparticles in the solid state. Adv Mater 2001;13:1699–701.
[59] Ingram RS, Hostetler MJ, Murray RW. Poly-hetero-ω-functionalized alkanethiolate-stabilized gold cluster compounds. J Am Chem Soc 1997;119:9175–8.

[60] Shaffer AW, Worden JG, Huo Q. Comparison study of the solution phase versus solid phase place exchange reactions in the controlled functionalization of gold nanoparticles. Langmuir 2004;20: 8343–51.
[61] Worden JG, Dai Q, Huo Q. A nanoparticle–dendrimer conjugate prepared from a one-step chemical coupling of monofunctional nanoparticles with a dendrimer. Chem Commun 2006: 1536–8.
[62] Wang WL, Xu IW, Lai YH. Bipyridinophane-containing conjugated polymers modulated with an intramolecular aromatic C–H/π interaction. J Polym Sci Part A Polym Chem 2006;44: 4154–64.